ejpmr, 2019,6(10), 26-38

SJIF Impact Factor 6.222

EUROPEAN JOURNAL OF PHARMACEUTICAL AND MEDICAL RESEARCH

www.ejpmr.com

Case Study

ISSN 2394-3211

EJPMR

EFFECT OF COPPER OXIDE NANOPARTICLES ON THE SPLEEN OF ADULT MALE ALBINO RAT AND THE POSSIBLE PROTECTIVE ROLE OF VITAMIN C HISTOLOGICAL STUDY

Aya Mostafa*, Somaya Abdel Alim, Gehad A Hammouda and Sara Abdel Gawad

Department of Histology and Cell Biology, Faculty of Medicine, Ain Shams University, Cairo, Egypt.

***Corresponding Author: Aya Mostafa**
Department of Histology and Cell Biology, Faculty of Medicine, Ain Shams University, Cairo, Egypt.
DOI: 10.20959/ejpmr201910-7274

Article Received on 26/07/2019 **Article Revised on 15/08/2019** **Article Accepted on 06/09/2019**

ABSTRACT

Background: Copper oxide nanoparticles (CuO NPs) have attracted attention mostly because of their antimicrobial and biocide properties. Despite their high application potential, there are various disadvantages of CuO NPs as they have potential toxic effects compared with other conventional metal oxide NPs. The primary target organs of CuO NPs are kidney, liver and spleen. **Aim of the work:** To assess the effect of two different doses of CuO NPs on the histological structure of the spleen of adult male albino rats and to evaluate the possible prophylactic role of vitamin C as an antioxidant. **Materials & methods:** Fifty adult male albino rats were divided randomly into three groups. Group I; served as control group, group II was divided into two subgroups: subgroup IIA; injected with 10 mg/kg CuO NPs intraperitoneal (IP) for seven days and subgroup IIB; injected with 25 mg/kg CuO NPs (IP) for seven days. Group III: received (IP) injection of 90 mg/kg vitamin C, then one hour later rats were subdivided into two subgroups. Subgroup IIIA; injected with CuO NPs in a dose of 10 mg/kg and subgroup IIIB; injected with 25 mg/kg CuO NPs (IP) for seven days. Spleen of all rats was dissected out and processed for histological and immunohistochemical study. Morphometric and statistical analysis were also performed. **Results:** Injection of CuO NPs induced structural changes in the spleen which were dose dependent. There was atrophy of the white pulp with predominance of the red pulp. Cells appeared vacuolated with darkly stained or fragmented nuclei. The blood sinusoids were dilated and congested. There was also significant increase in caspase-3 positive cells compared to the control group. However, prophylaxis with vitamin C illustrated good improvement in the histological picture of the spleen of subgroup IIIA but minimal protective effect was observed in subgroup IIIB. **Conclusion and recommendations:** CuO NPs induced structural changes in the splenic architecture and this response was augmented with increasing the dose. In addition, vitamin C alone was not efficient in preventing CuO NPs cytotoxicity especially in high dose. More investigations should be done to fully elucidate the prophylactic effect of vitamin C combined with other antioxidants to protect the spleen from CuO NPs toxicity.

KEYWORDS: Copper oxide nanoparticles (CuO NPs), spleen, Lymphocytes, Macrophages.

INTRODUCTION

Nowadays, scientific research on nanoparticles (NPs) has shown a great and rapid growth due to their wide applications in various fields, including electronics, cosmetics, food industry and medicine. Therefore, there is increasing probability for human and environmental contact with these nanomaterials.[1]

Based on the sources used, there are mainly four types of NPs as mentioned by *Vance et al;*[2], metal oxide NPs, metallic NPs, polymeric NPs and Carbon based NPs.

Currently, interest has especially increased in metal oxide NPs as they exhibit unique chemical and physical properties. There are several types of metal oxide NPs such as copper oxide, zinc oxide, titanium oxide and magnesium oxide.[3]

Copper oxide (CuO) is a semiconductor metal with unique optical, electrical and magnetic properties. It has been used for various applications, such as the development of supercapacitors, near-infrared filters, in magnetic storage media, sensors, catalysis and semiconductors.[4]

Although CuO nanoparticles (CuO NPs) have proved their use in biomedical applications; they have potential toxic effects compared with other conventional metal oxide NPs. The main toxicity process relies on the increased production of reactive oxygen species.[5] The primary target organs of CuO NPs are kidney, liver and spleen.[6]

Spleen is the largest secondary lymphoid organ with a complex vascular and cellular organization. The spleen induce immune response against blood antigens, and

defend against invading bacteria, fungi, viruses and other infective agents. The spleen represents an important clearance site for NPs due to its high blood flow and loose capillaries.[7]

Exogenous antioxidants like vitamin C, vitamin E, and beta carotene or vitamin A are among the most widely studied dietary antioxidants. Vitamin C is considered the most important water-soluble antioxidant in extracellular fluids.[8] Vitamin C has the ability to reduce and neutralize reactive oxygen species. It is a cofactor for enzymes involved in regulating hormone biosynthesis, and regenerating other antioxidants e.g. vitamin E. Moreover, it has a role in detoxifying the body from heavy metals.[9]

Hence, the objective of this study was to assess the effect of exposure to CuO NPs, in two different doses, on the splenic structure of male adult albino rats and the possible prophylactic role of vitamin C was investigated.

MATERIALS AND METHODS

Animals

Fifty male adult albino rats of average weight 170-200 gm were purchased and maintained in animal house of Medical Research Unit, Faculty of Medicine, Ain Shams University. Animals were housed in plastic cages with mesh wire covers and were given rat chow and water *ad libitum*. All animal procedures were performed according to the general guidelines for the care and use of laboratory animals and approved by the animal ethical committee at Faculty of Medicine, Ain Shams University.

Characterization of CuO NPs

Copper oxide NPs were purchased from NanoTech Egypt for Photo-Electronics, 6th of October city, Giza, Egypt, as a black powder of size ≈ 30 ± 5 nm. CuO NPs characterization was done using transmission electron microscope (TEM) at the Regional Center for Mycology and Biotechnology, Al-Azhar University (JEOL-JEM-1010), to assess their shape, size and aggregation state. This was done by forming a suspension of CuO NPs in distilled water which was put in sonicator for 10 minutes. Then it was deposited on carbon coated copper grids and allowed to dry at ambient temperature.**[10]** Particles size were measured in different fields (60000 X) using an Image software package (US National Institutes of Health, Bethesda, Maryland, USA), installed on the TEM.

Experimental design

The animals were randomly divided into three groups:

- **Group I (control group, n=10):** subdivided into two equal subgroups:
  - **Subgroup IA:** received 0.5 ml of distilled water (DW) by intraperitoneal injection (IP) daily for 7 successive days.
  - **Subgroup IB:** received (IP) injection of 90 mg/kg vitamin C one hour before receiving 0.5 ml of DW by IP injection, daily for 7 successive days.
- **Group II (n=20):** subdivided into two equal subgroups:
  - **Subgroup IIA:** received (IP) injection of CuO NPs in a dose of 10 mg/kg suspended in 0.5 ml DW, daily for 7 successive days.**[11]**
  - **Subgroup IIB:** received (IP) injection of CuO NPs in a dose of 25 mg/kg suspended in 0.5 ml DW, daily for 7 successive days "modified from **Anreddy *et al*;**[12]".
- **Group III (n=20):** subdivided into two equal subgroups.
  - **Subgroup IIIA:** received (IP) injection of 90 mg/kg vitamin C one hour before receiving (IP) injection of CuO NPs in a dose of 10 mg/kg suspended in 0.5 ml DW, daily for 7 successive days.
  - **Subgroup IIIB:** received (IP) injection of vitamin C in a dose of 90 mg/kg one hour before receiving CuO NPs in a dose of 25 mg/kg B.W suspended in 0.5 ml DW by IP injection, daily for 7 successive days.

Histological and immune-histochemical studies

For LM study; half of the spleen specimens were fixed in 10% buffered formalin, dehydrated, cleared and embedded in paraffin. Serial 5 µm sections were stained with hematoxylin and eosin (H&E) and Immune-histochemical staining using avidine-biotin peroxidase technique for demonstration of caspase-3.**[13]** Positive control were sections of rat testis. Negative control sections were processed according to the same protocol except for omitting the primary antibody. The primary antibody used was polyclonal rabbit anti-rat caspase-3 antibody and the secondary antibody was goat anti-rabbit peroxidase-conjugate secondary antibody. Both antibodies came from Sigma-Aldrich Company in the USA but they were purchased from Labvision company in Egypt.

For transmission electron microscope (TEM) examination; other half of the spleen specimens were cut into small pieces ($1mm^3$) and fixed in 2.5% gluteraldhyde, then 1% osmium tetroxide, dehydrated and embedded in epoxy resin. Ultrathin sections (60-80 nm) were mounted on copper grids and stained with uranyl acetate and lead citrate **(14)** to be examined by TEM (JEM-1200; Jeol, Akishima-Shi, Tokyo, Japan) at the the Regional Center for Mycology and Biotechnology, Al-Azhar University.

Morphometric and statistical studies

Analysis of the sections were done using an image analyzer (Leica Q win V.3 program) installed on a computer in the Histology and cell biology Department, Faculty of Medicine, Ain Shams University. The PC was connected to a Leica DM2500 microscope with built-in camera (Leica Microsystems GmbH, Ernst-Leitz-StraBe, Wetzlar, Germany). Five sections from five different rats

of each subgroup were examined (n=5). From each section, five different captured non-overlapping fields were taken.

Five different readings from every captured photo were counted and mean was calculated for each specimen. Measurements were taken by an independent observer blinded to the specimens' details to perform an unbiased assessment. The mean number of caspase-3 positive cells per high power field (×400) was calculated and expressed as mean ± SD. Statistical analysis was performed using statistical package for the social sciences (SPSS), software program, version 20 (IBM corporation, Armwork, North castle, Westchesten Country, New York, USA).

Statistical difference among subgroups for each parameter was determined using two-way analysis of variance (ANOVA) and post-Hoc least significance difference (LSD). The significance of the data was determined by the P value; P values ≤ 0.05 were considered statistically significant.

RESULTS

Characterization of CuO NPs

TEM examination of CuO NPs revealed tiny electron dense particles of relatively similar size range. They appeared nearly rounded, solid and non-porous. Some CuO NPs tend to join together and form aggregates **(Fig. 1)**.

Light microscopic and morphometric results of the spleen

Histological examination of H&E stained sections of subgroup IA & subgroup IB of the control group revealed the same histological picture. The spleen showed thin regular splenic capsule. The parenchyma of the spleen was formed of white pulp and red pulp separated by marginal zone. The white pulp was formed of lymphoid follicles and PALS. The lymphoid follicles appeared with germinal centers and eccentric follicular arterioles **(Fig.2a)**. The lymphocytes in the white pulp were heavily populated and their nuclei appeared darkly stained with eccentric follicular arteriole **(Fig.3a)**. The red pulp was formed of cords of cells (cells of Billroth) separated by blood sinusoids that was lined by flat endothelial cells. Macrophages laden with hemosiderin granules were seen in the sections **(Fig.4a)**. Sections of subgroup IIA showed patchy histological changes. Thickened corrugated capsule could be seen **(Fig.2b)**. Atrophy of the white pulp with predominance of congested red pulp were observed. Some follicles appeared small, irregular in shape with ill-defined marginal zone **(Fig.2b &2c)**. In addition, the wall of the follicular artery appeared thickened and vacuolated compared to the control. Lymphocytes appeared widely separated and fragmented irregular nuclei were seen in some cells **(Fig.3b)**. The red pulp revealed dilated congested blood sinusoids with extravasated RBCs in between. Cells laden with hemosiderin granules were also detected. In addition, fragmented nuclei were detected in some cells **(Fig.4b)**. In subgroup IIB, marked atrophy of the white pulp with predominance of the red pulp were prominently observed. Lymphoid follicles appeared small, distorted and irregular with ill-defined marginal zone. Numerous vacuoles were recognized in the interstitium. The splenic capsule appeared thickened **(Fig.2d)**. The wall of the follicular artery appeared highly thickened and vacuolated. The cells in the white pulp revealed deeply stained nuclei of the lymphocytes. In addition, small dark particles were seen intracellular and extracellular (**Fig. 3c)**. Regarding the red pulp, the cells were widely separated, the nuclei showed different stages of degeneration (pyknosis, karyorrhexis and karyolysis). Moreover, vacuolated cells were detected in the red pulp and were separated by congested dilated blood sinusoids. However, hemosiderin laden macrophages were unexpectedly less than these in subgroup IIA **(Fig.4c)**. However, subgroup IIIA revealed a histological picture of the spleen more or less comparable to the control group. The spleen was covered by thin regular capsule. The parenchyma was formed of white pulp and red pulp with well demarcated marginal zone **(Fig.2e)**. The wall of the follicular artery was slightly thickened compared to the control group. The lymphoid follicles appeared formed of closely packed lymphocytes with darkly stained nuclei, however few lymphocytes showed fragmented nuclei **(Fig.3d)**. The red pulp appeared composed of cords of Billroth separated by blood sinusoids. Few vacuolated cells and hemosiderin laden macrophages were detected. Some blood sinusoids appeared dilated **(Fig.4d)**. In subgroup III B, the white pulp revealed distorted lymphoid follicles with ill-defined marginal zone. The splenic capsule appeared slightly thickened and corrugated **(Fig.2f)**. The wall of the follicular artery was moderately thick compared to the control group. The lymphocytes in the white pulp appeared with darkly stained nuclei, while other cells appeared with pale degenerating nuclei. In addition, some cells appeared vacuolated **(Fig. 3e)**. The blood sinusoids in the red pulp appeared congested and some were dilated. The cells in between the blood sinusoids have vesicular nuclei, dark nuclei or pale degenerating nuclei **(Fig.4e)**.

In immnohistochemical analysis for caspase-3, subgroups IA and IB showed few scattered immuno-reactive cells with non-significant difference ($P > 0.05$) between both of them **(Fig.5a)**. However, subgroups IIA & IIB showed significant increase ($P < 0.05$) in the mean number of caspase-3 immuno-reactive cells compared to subgroup IA (control group) **(Fig. 5b & 5c respectively) (Table 1)**. Prophylaxis with vitamin C led to significant decrease ($P < 0.05$) in the mean number of caspase-3 immune-reactive cells in subgroup IIIA **(Fig. 5d)** and subgroup IIIB (**Fig.5e)** in comparison with subgroups IIA & IIB respectively **(Table 1)**. Additionally, subgroups IIIA & IIIB showed non-significant difference ($P > 0.05$) compared to the subgroup IA (control group) **(Table1)**.

Transmission electron microscope results

Examination of the spleen sections of the control group illustrated the white pulp which is formed mainly of closely packed lymphocytes with different sizes and their nuclei appear regular, oval or rounded and moderately electron dense. Fibroblasts could be identified within connective tissue septa **(Fig.6a)**. Many different cells including RBCs, lymphocytes, macrophages, plasma cells and eosinophils were noticed in the red pulp. Macrophages appeared with kidney shaped indented nuclei and the cytoplasm showed many lysosomes. Macrophages engulfing RBCs were seen in some sections **(Fig.7a)**. Blood sinusoids appeared in between the cords of cells in the red pulp and were lined by flat endothelial cells **(Fig.7b)**. However, examination of the spleen sections of subgroup IIA revealed depletion of cells in the white pulp. Many plasma cells were also observed. Some nuclei appeared shrunken, deeply stained and others revealed irregular nuclei with condensation and margination of chromatin. In addition, few RBCs were observed in between the cells **(Fig. 6b)**. A clear finding in the red pulp was the presence of plenty of plasma cells and macrophages. Furthermore, some nuclei appeared irregular in shape with condensation and margination of chromatin **(Fig. 7c)**. Sections of subgroup IIB revealed numerous neutrophils with their characteristic multilobed nuclei. Some cells appeared with degenerating nuclei and vacuolated cytoplasm. Other nuclei revealed condensation and margination of chromatin with perinuclear space **(Fig. 6c)**. In addition, some electron dense granules and some vacuoles were observed in the interstitium **(Fig. 6c & 6d)**. Some sections showed massive deposition of collagen fibers accompanied with fibroblasts having irregular electron dense nuclei **(Fig. 6d)**. In the red pulp, some sections revealed the presence of megakaryocytes with their characteristic demarcation zones and electron dense granules **(Fig. 7d)**. Prophylaxis with vitamin C in subgroup IIIA showed noticeable improvement in the histological structure of the spleen in comparison to subgroup IIA. The white pulp revealed lymphocytes with more or less regular nuclei. However, few lymphocytes showed margination and condensation of chromatin and others revealed small electron dense degenerating nuclei **(Fig. 6e)**. The red pulp showed congested blood sinusoids lined by flattened endothelial cells and surrounded by reticular cells. Macrophages with indented eccentric nuclei and numerous lysosomes were detected. In addition, small electron dense particles and aggregates were seen in the interstitium **(Fig. 7e)**. In subgroup III B, minimal improvement was recorded in the histological structure of the spleen compared to subgroup II B. The white pulp revealed some lymphocytes with irregular nuclei and chromatin condensation and margination, while others showed small electron dense nuclei with disrupted nuclear membrane. Macrophages were also observed in the white pulp. Moreover, some electron dense particles were seen intracellular and extracellular **(Fig.6f)**. On the other hand, the red pulp showed different blood cells including eosinophils, macrophages and lymphocytes. Numerous electron dense particles were seen in the interstitium **(Fig. 7f)**.

Table (1): showing the mean number of caspase-3 positive cells in different subgroups.

	Subgroup IA	**Subgroup IIA**	**Subgroup IIB**	**Subgroup IIIA**	**Subgroup IIIB**
Caspase 3 positive cells/HPF	11.40 ± 2.69	75.06 ± 18.2 (* ▲ Δ)	95.33 ± 19.6 (* ▲ Δ)	15.20 ± 7.30 **(♣ O)**	17.06 ± 9.42 **(♣ O)**

***** Significant difference from subgroup IA.
♣ Significant difference from subgroup IIA.
O Significant difference from subgroup IIB.
▲ Significant difference from subgroup IIIA.
Δ Significant difference from subgroup IIIB.

Legends

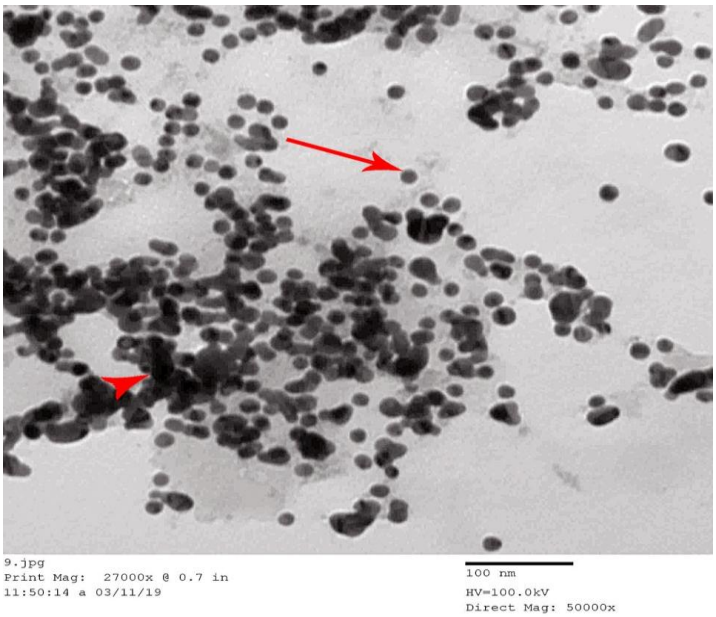

Figure (1): An electron micrograph of CuO NPs showing rounded, non-porous, electron dense particles (↑). Notice the presence of nanoparticle aggregations (►).

(TEM x 50000)

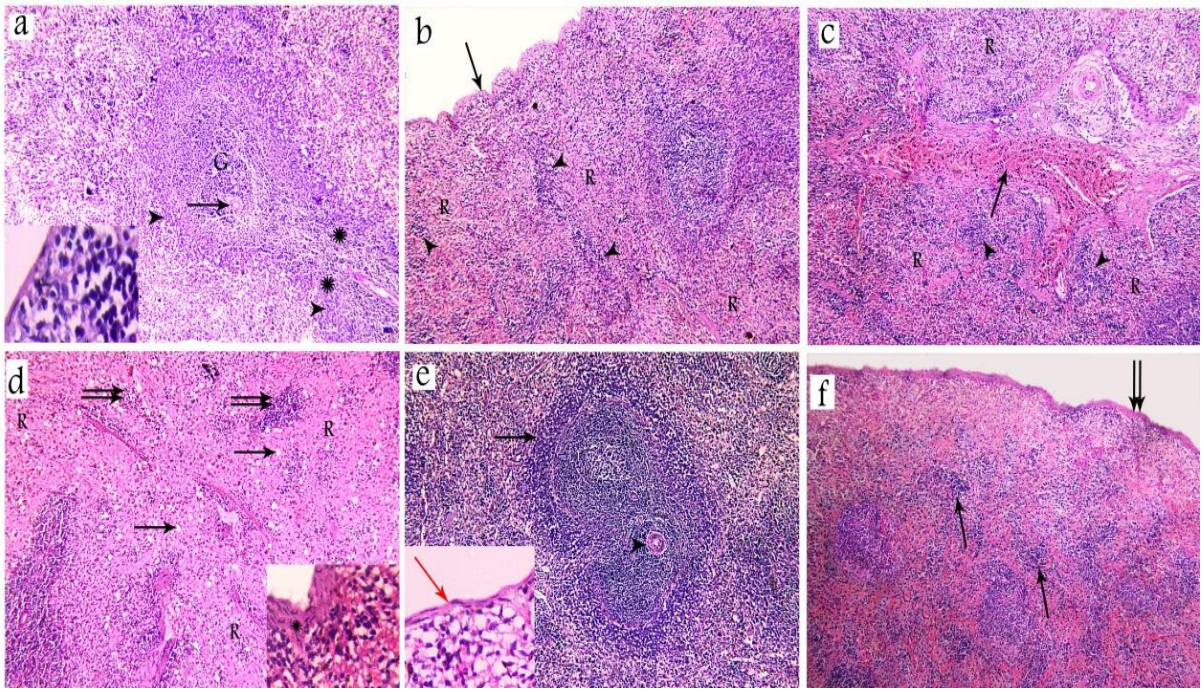

Figure (2): (2a): Subgroup IA showing splenic follicle with pale germinal center (G) and eccentric follicular artery (↑). Peri-arterial lymphatic sheath (*) surrounding central arteriole was seen. Notice the marginal zone (►) separating the white pulp from the surrounding red pulp. The inset shows regular splenic capsule. (2b): Subgroup IIA showing corrugated splenic capsule (↑). Notice the predominance of red pulp (R) and atrophy of the white pulp (►). (2c): Subgroup IIA showing congested dilated blood vessel (↑). Predominance of the red pulp (R) with no demarcation between the white (►) and red pulp. (2d): Subgroup IIB showing predominance of the red pulp (R). The lymphoid follicles appeared small irregular with ill-defined marginal zone (↑↑). Notice the presence of numerous vacuoles (↑). The inset shows thickened splenic capsule. (2e): Subgroup IIIA showing well demarcated splenic follicles with eccentric follicular artery (►) and well-defined marginal zone (↑). The inset shows thin regular splenic capsule (red arrow). (2f): Subgroup IIIB showing distorted lymphoid follicles with ill-defined marginal zone (↑). Notice the slightly thickened corrugated splenic capsule (↑↑).

(H&E x 100, Inset x 400)

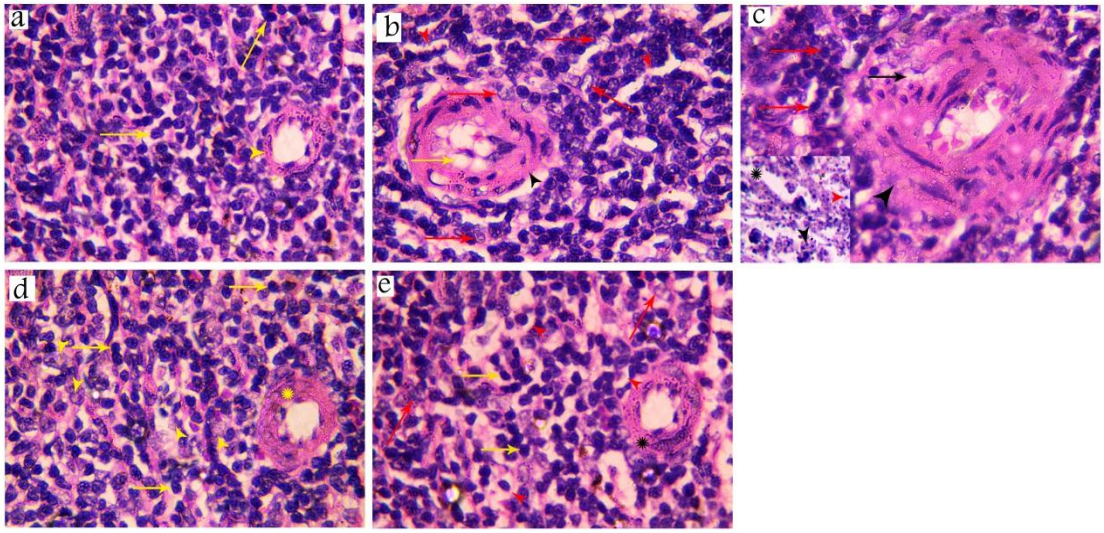

Figure (3): (3a): Subgroup IA showing part of a lymphoid follicle having lymphocytes with deeply stained nuclei (yellow arrow) and eccentric follicular artery (yellow arrowhead). (3b): Subgroup IIA showing wide intercellular spaces (↑). Fragmented nuclei were seen in some cells (red arrow). Notice thickening of the follicular artery wall (►) with vacuolations (yellow arrow). (3c): Subgroup IIB showing thickened wall of the follicular artery (►) with vacuolations (black arrow). Notice the deeply stained nuclei of lymphocytes (red arrow). The inset reveals numerous small dark particles intracellular (black arrowhead) and extracellular (red arrowhead) with wide intercellular spaces (*). (3d): Subgroup IIIA showing lymphocytes with deeply stained nuclei (yellow arrow). Few cells show fragmented nuclei (yellow arrowhead). Notice the follicular artery (*) with slightly thickened wall. (3e): Subgroup IIIB showing lymphocytes with darkly stained nuclei (yellow arrow). Some cells reveal pale degenerating nuclei (red arrow) and others appear with vacuolated cytoplasm (red arrowhead). Notice slightly thickened follicular artery (*).

(H&E x 1000, Inset x 400)

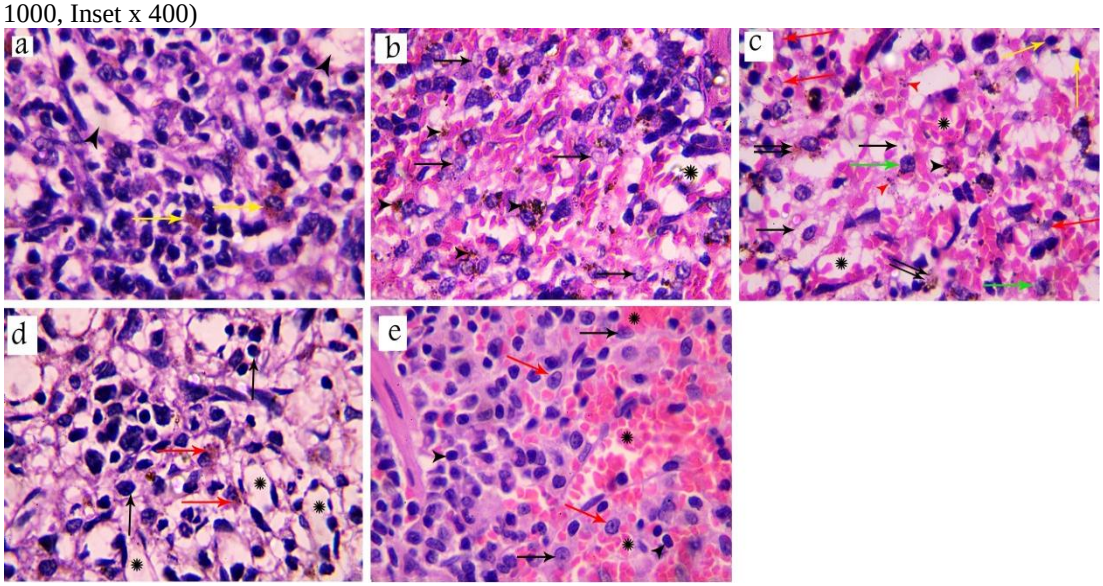

Figure (4): (4a): Subgroup IA showing the red pulp formed of splenic cords of Billroth and blood sinusoids (►) lined by flat endothelial cells. Notice the presence of macrophage laden with hemosiderin granules (yellow arrow). (4b): Subgroup IIA showing congested dilated blood sinusoid (*). Hemosiderin granules laden cells could be seen (►). Notice fragmented nuclei in some cells (↑). (4c): Subgroup IIB showing vacuolated red pulp (↑) and dilated congested blood sinusoids (*). Small dark particles are seen intracellular (►) and extracellular (red arrow head). In addition, haemosiderin deposits within cells of the red pulp are observed (↑↑). Notice pyknosis (yellow arrow), karyorhexis (green arrow) and karyolysis (red arrow) of the nuclei. (4d): Subgroup IIIA showing blood sinusoids (*) lined by flattened endothelial cells. Vacuolated cells (↑) and hemosiderin laden macrophages (red arrow) could also be noticed. (4e): Subgroup IIIB showing dilated and congested blood sinusoids (*). Lymphocytes reveal either darkly stained nuclei (►), vesicular nuclei (red arrow) or pale degenerating nuclei (↑).

(H&E x1000)

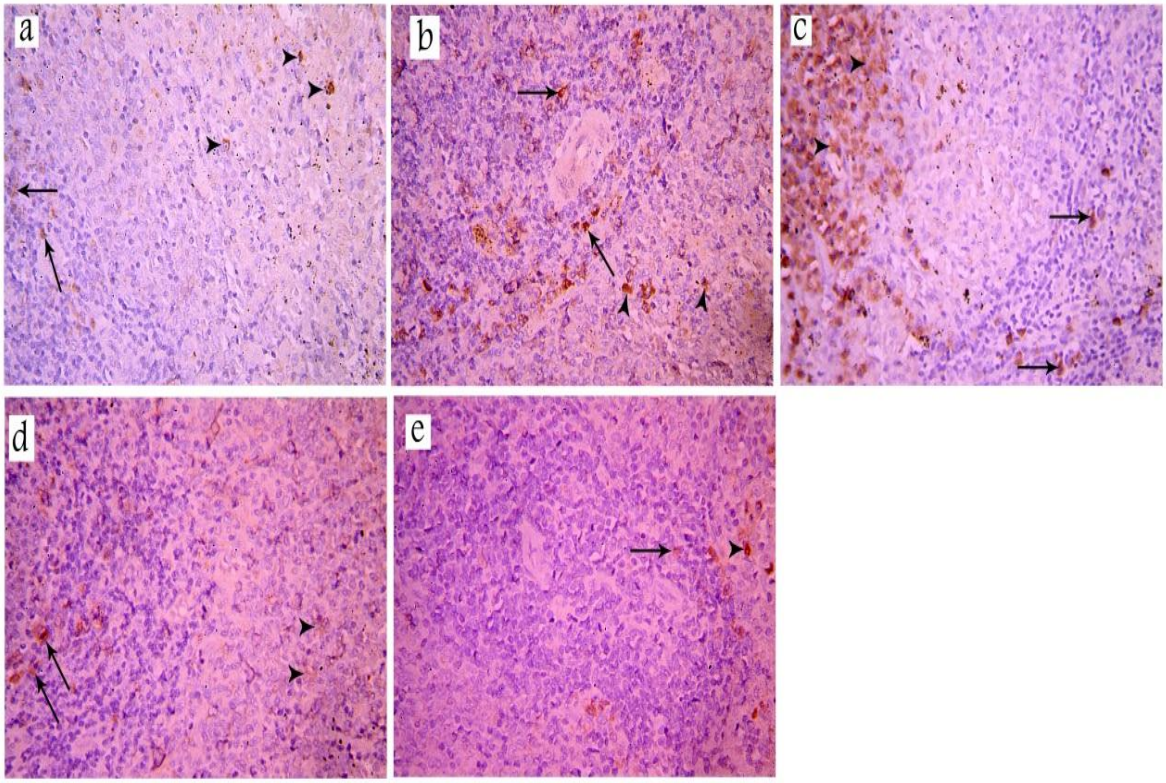

Figure (5): (5a): Subgroup IA showing few scattered cells with weak immuno-histochemical reaction for caspase-3 in the white pulp (↑) and red pulp (►). (5b): Subgroup IIA showing numerous scattered cells with strong immuno-histochemical reaction for caspase-3 in the white pulp (↑) and the red pulp (►). (5c): Subgroup IIB showing strong immuno-histochemical reaction for caspase-3 in few cells of the white pulp (↑) and numerous cells in the red pulp (►). (5d): Subgroup IIIA showing few scattered cells with weak immuno-histochemical reaction for caspase-3 in the white pulp (↑) and the red pulp (►). (5e): Subgroup IIIB showing weak immuno-histochemical reaction for caspase-3 in few dispersed cells in the white pulp (↑) and the red pulp (►).

(Avidin-Biotin peroxidase technique x 400)

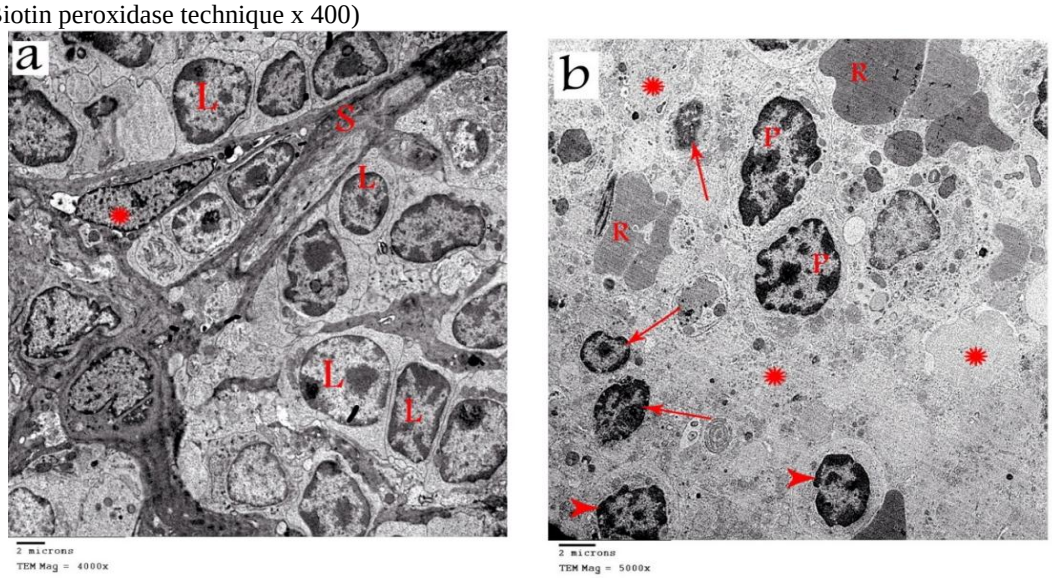

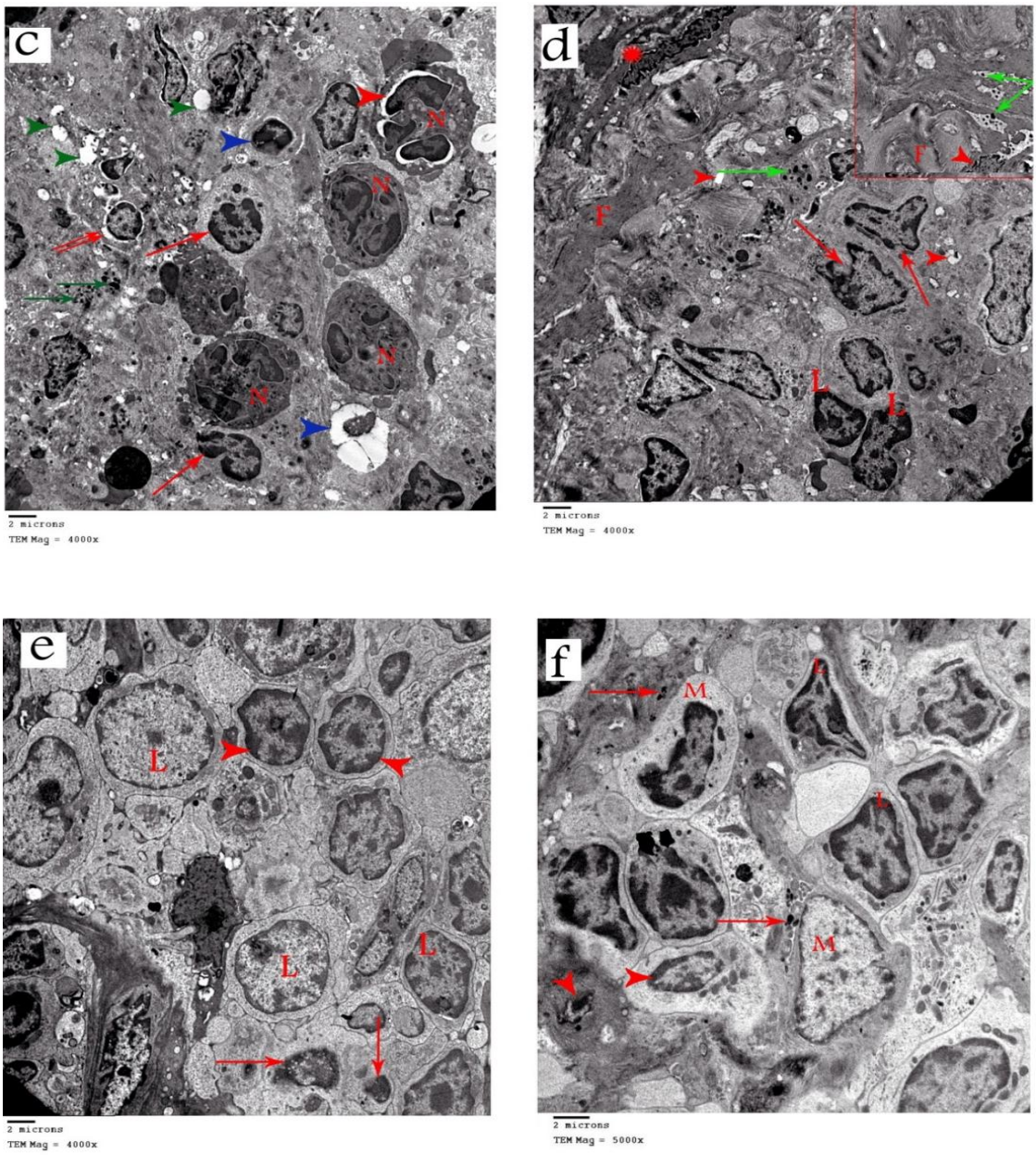

Figure (6): (6a) Subgroup IA showing the white pulp which appear formed mainly of closely packed lymphocytes (L). Notice the presence of fibroblast (*) within the septum (S). (6b): Subgroup IIA showing depletion of cells (*) of the white pulp. Some nuclei appear small and deeply stained (↑) and other nuclei reveal condensation and margination of chromatin (►). Notice the presence of plasma cells (P) and RBCs (R). (6c): Subgroup IIB showing the cells of white pulp revealing condensation and margination of chromatin (red arrow) with perinuclear space (↑↑). Few cells appear with degenerated electron dense nuclei (blue arrowhead). Neutrophils (N) with multilobed nuclei and perinuclear space (red arrowhead) are seen. Notice the presence of some vacuoles (green arrowhead) and electron dense small particles (green arrow) in the interstitium. (6d): Subgroup IIB showing increased collagen fibers deposition (F) in the interstitium accompanied with fibroblast with irregular nuclear membrane (*). Lymphocytes (L) reveal condensation and margination of chromatin. Some cells appear with disrupted nuclear membrane (red arrow). The interstitium illustrate vacuolations (►) and electron dense granules (green arrow). (6e): Subgroup IIIA showing the white pulp, most of the lymphocytes appear with regular nuclear membrane (L). However, some lymphocytes show margination and condensation of chromatin (►) and others have small electron dense nuclei (↑). (6f): Subgroup IIIB showing the white pulp with some lymphocytes (L) with irregular nuclei and condensation and margination of chromatin. Other lymphocytes show small electron dense nuclei with disrupted nuclear membrane (►). Notice the presence of macrophage (M) and small electron dense particles (↑).

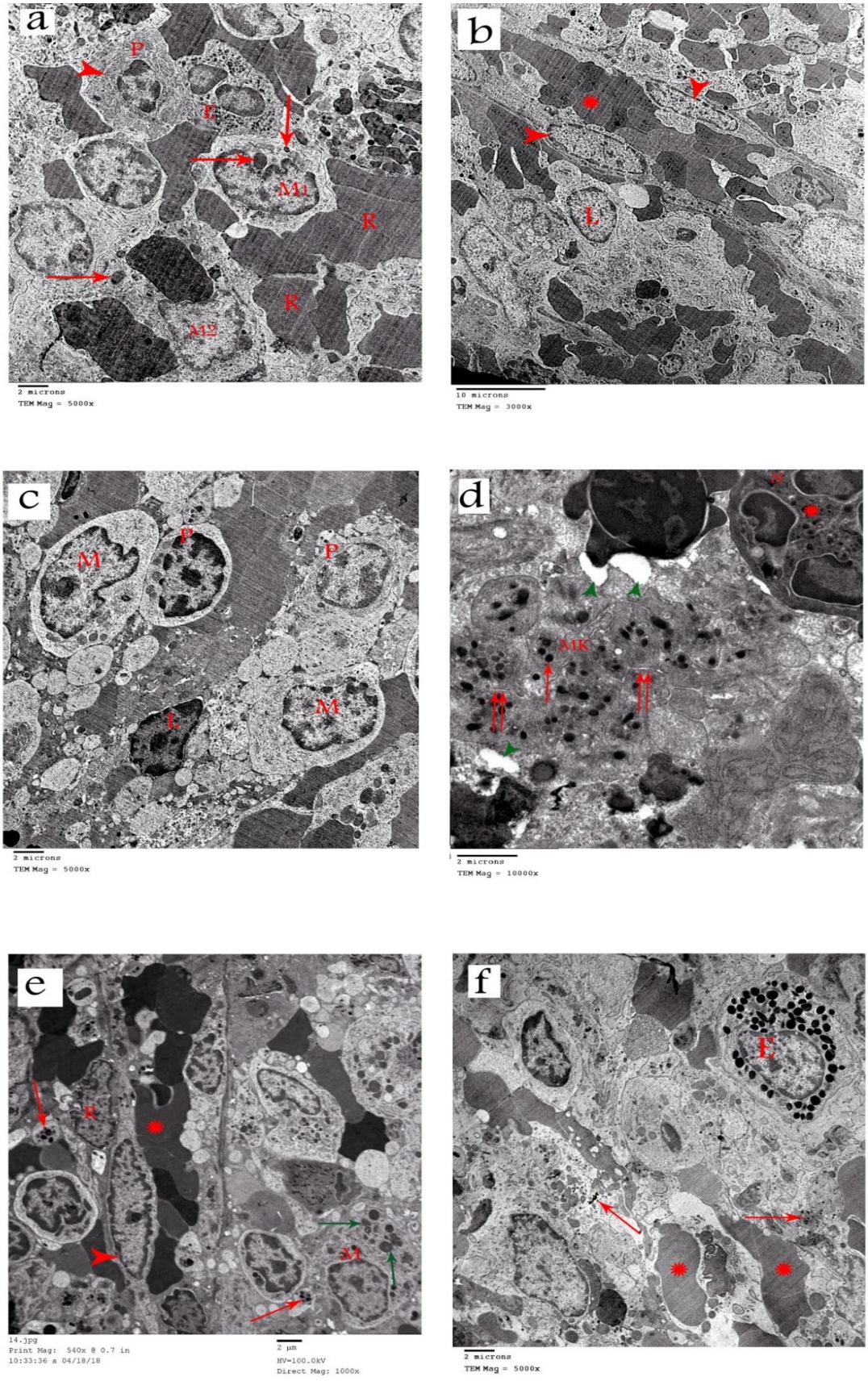

Figure (7): (7a): Subgroup IA showing the red pulp formed of different cell types including plasma cells (P) with well-developed rER (►), eosinophils (E) and RBCs (R). Macrophages (M1) and macrophage engulfing RBC (M2) can be observed in the red pulp. Lysosomes in the cytoplasm of macrophages could be identified (↑). (7b): Subgroup IA showing a blood sinusoid lined by flat endothelial cells (►) with RBCs (*) in its lumen.

Lymphocytes (L) could also be seen. (7c): Subgroup IIA showing the red pulp containing macrophages (M), plasma cells (P) and lymphocyte (L) with chromatin condensation and margination. (7d): Subgroup IIB showing megakaryocyte (MK) with its characteristic demarcation zones (↑↑) and containing electron dense granules (↑). Neutrophil (N) with multilobed nucleus and electron dense granules (*) in its cytoplasm can be observed. Notice the vacuoles (►) in the interstitium. (7e): Subgroup IIIA showing the red pulp with a blood sinusoid (*) that appear congested, lined by flattened endothelial cells (►) and surrounded by reticular cell (R). Macrophages (M) with cytoplasmic lysosomes (green arrow) can be observed. Notice small electron dense particles (red arrow). (7f): Subgroup IIIB showing the red pulp containing eosinophil (E) with its characteristic granules. Notice few small electron dense particles (↑). RBCs (*) are seen in between the cells of the red pulp.

DISSCUSION

Copper oxide NPs have attracted an increased attention for biomedical and industrial applications. They also show significant antibacterial and biocidal activities **(1)**. However, this wide-scale use of CuO NPs makes humans more prone to their exposure and their potential adverse health effects.[15]

Kidney, liver and spleen are considered the primary target organs for CuO NPs as stated by ***Dumková et al;***.[16] Therefore, the present experiment was designed to study effects of CuO NPs on the histological structure of the spleen as many studies showed their toxic effects on the liver and kidneys, but less were concerned about their effect on the spleen.

Characterization of CuO NPs was performed by TEM and it showed that they have rounded shape, size range of 25-35 nm with solid characteristics. This result is consistent with those of ***Lai et al;***[17] and ***Yokohira et al;***[18] ***Yokohira et al;*** studied the lung toxicity caused by intratracheal instillation of 33 nm CuO NPs and found that NPs caused severe acute toxicity, severe inflammatory changes, neutrophil infiltration and even acute death.[18]

Also, the study done by ***Anreddy et al;*** **(12)** indicated that CuO NPs of size <50 nm; nearly similar to the size used in the current study; caused severe toxicological effects on the liver of experimental rats.

In the current study, group II (subgroups IIA & IIB) showed histopathological changes in the splenic architecture caused by CuO NPs. These changes were more extensive with increasing the dose of CuO NPs in subgroup II B. Both H&E and TEM examination of subgroups IIA & IIB showed small particles scattered intracellularly and extracellularly in the white and red pulps which are most probably CuO NPs. This finding was consistent with the study of ***Sizova et al;***[19] which showed that three hours after the injection of 2 mg/kg Cu NPs into the muscle, these nanoparticles were observed in the vascular zone of the liver and in the cytoplasm of Kupffer liver cells.

In the present experiment, TEM study of both subgroups IIA & IIB revealed macrophages engulfing small electron dense particles in their cytoplasm which are most likely CuO NPs. This is consistent with other studies which proved that NPs uptake in the spleen occurred mainly by marginal zone macrophages.[20]

Unexpectedly, macrophages were observed prominently in subgroup II A which received low dose of CuO NPs than in subgroup IIB which received high dose of NPs. This is most probably due to the toxic effect of high dose of CuO NPs that will be phagocytosed by macrophages which in turn will cause oxidative stress leading to cell death. This comes in accordance with ***Wang et al.*** [21] who stated that ZnO NPs led to macrophage death due to release of zinc ions inside cells which in turn led to over generation of intracellular ROS, leakage of plasma membrane, dysfunction of mitochondria, and finally cell death.

After NPs are engulfed by macrophages, these NPs induce an inflammatory reaction and stimulate secretion of pro-inflammatory cytokines and interleukins as IL-1β and IL-18.[22] This can explain the presence of numerous immune cells including plasma cells, neutrophils, eosinophils and macrophages which were noticed in TEM examination of subgroups IIA & IIB.

In the present study, H &E stained sections of subgroup IIA & IIB revealed depletion of cells with atrophy of the white pulp. The follicles appeared small, irregular in shape with ill-defined MZ. This was confirmed by TEM sections in which depletion of cells with wide intercellular spaces were observed. This is consistent with ***Mazen et al;*** **(23)** who studied the toxicity of silver nanoparticles (Ag NPs) on rat spleen. They attributed these findings to cytotoxicity and apoptosis induced by NPs.[23] Moreover, ***Y Yu et al;***[24] stated that CuO NPs induced dose dependent toxicity and oxidative stress in rats due to increased ROS and decreased levels of antioxidants which could explain the observed cell depletion and splenic follicles atrophy.

Regarding nuclear changes that occurred in current study, karyorrhexis, karyolysis & pyknosis were observed in both subgroups IIA &IIB. This denotes fragmentation of the nucleus with irreversible condensation of the chromatin. In accordance with the present results, ***Kumar et al;***[25] and ***Cholewińska et al;***[26] mentioned that variable degrees of necrotic cellular injury, karyolysis and pyknosis occurred following the use of NPs.

In addition, margination and condensation of heterochromatin with a perinuclear space and disrupted nuclear membrane were detected in TEM of subgroups that received CuO NPs only. This comes in harmony with ***Abu-Dief et al;***[27] who used titanium dioxide NPs and they reported irregular disrupted nuclear membrane with condensation and margination of heterochromatin in liver cells. ***Smetana et al.,***[28] reported that cells undergoing apoptosis show fragmentation of their nuclei, condensation and margination of their heterochromatin representing non-proliferating, terminal pre-apoptotic cells just before the loss of the nucleus. Therefore, all the nuclear changes seen in our study indicate cell apoptosis which is most probably due to ROS production inside the cell.

This was documented by significant increase in the number of caspase-3 immuno-reactive cells in both subgroups IIA & IIB in comparison to the control group. This comes in harmony with ***Lai et al;***[17] who found apoptotic cells after intranasal instillation of CuO NPs in lung of rats and mice.

Moreover, cytoplasmic vacuolations were significant in subgroups IIA & IIB which is a well-known morphological phenomenon observed in cells after exposure to bacterial or viral pathogens as well as to various natural and artificial low-molecular-weight compounds and nanoparticles. It often accompanies cell death; however, its role in cell death processes remains unclear.[29]

According to ***Schrand et al;***[30], they attributed cytoplasmic vacuolations to hydropic degeneration that occurs as a result of ion and fluid homeostasis leading to an increase of intracellular water which is facilitated by the disruption of the plasma membrane.

Moreover, subgroups IIA & IIB revealed vacuolations in the endothelial cells lining the follicular artery with congested dilated splenic sinusoids and extravasated RBCs. This is consistent with ***Trickler et al;***[31] who stated that Ag NPs can induce inflammation to micro-vessel endothelial cells of the blood brain barrier with increasing permeability of the biological barrier and reducing the integrity of endothelial cell layer.

Additionally, the present study revealed dilated congested splenic sinusoids which is most probably due to portal hypertension or heart failure as CuO NPs were injected intraperitoneally. This did not affect the spleen alone but also affected liver, kidney and heart. This comes in harmony with ***Cho et al.***[32] who studied the toxicity of Ag NPs after intraperitoneal injection. Congestion in the liver and the spleen and thrombus in the heart were found. Therefore, dilatation and congestion of splenic sinusoids could be due to toxic effect of CuO NPs on the endothelial cells or due to other organs affection.

Regarding the red pulp, it was predominant in the histological sections of the spleen with the two given doses of CuO NPs in subgroups IIA & II B. This may be caused by pathological conditions, such as portal hypertension, cardiac failure, or extramedullary hematopoiesis. Extramedullary hematopoiesis most probably occurred as a result of inflammatory mediators released in response to CuO NPs. This can explain the presence of megakaryocytes in TEM examination of subgroup IIB. Therefore, as the dose increases, the level of inflammation increases, leading to increased red pulp area in the spleen which was more prominent in subgroup IIB. This comes also in harmony with ***Magaye et al:***[33], who outlined that nickel NPs led to extramedullary hematopoiesis and red pulp predominance in the spleen.

In the current study, vitamin C was used as a prophylaxis with CuO NPs. Good improvement was shown in subgroup IIIA that received 10 mg/kg of CuO NPs, but its effect was limited in subgroup IIIB that administered 25 mg/kg. In subgroup IIIA, the white pulp follicles were well demarcated and only few lymphocytes showed fragmented nuclei with slightly congested red pulp. Also, few scattered cells revealed caspase-3 immuno-histochemical reaction with non-significant difference compared to the control group. This comes in harmony with ***Fukui et al;***[34] who indicated that the oxidative stress and inflammatory response induced by ZnO NPs were prevented by co-treatment with vitamin C in human lung carcinoma A549 cells.

Fukui et al; also mentioned that vitamin C has the ability to chelate the extracellular Zn ions and form a complex which is readily taken up into the cell. Even if the intracellular Zn ions level is high, cytotoxicity might be reduced because Zn–Ascorbic acid complex is stable.[34] Moreover, vitamin C showed a significant role in inhibiting the reproductive toxicities induced by Ni NPs in male rat testes.[35]

On the other hand, administration of vitamin C in subgroup IIIB which received high dose of CuO NPs revealed partial protective effect. This comes in harmony with ***Diab et al.***[36] who studied the effect of vitamin C in improving neurotoxicity induced by ZnO NPs in rats. Rats treated by vitamin C showed partial ameliorative effect against ZnO NPs induced neurotoxicity.

So, it is concluded that vitamin C alone is not efficient to protect against CuO NPs cytotoxicity. This is consistent with ***Privalova et al;***[11] who used bioprotective complex formed of multi-vitamin multi-mineral preparation, some amino acids and fish oil to decrease CuO NPs induced hepatotoxicity and nephrotoxicity in rats. This bioprotective complex reduced systemic and target organ toxicity, as well as the genotoxicity of these NPs.

Regarding the antioxidant activity of vitamin C, it has the ability to donate a hydrogen atom and form a

relatively stable ascorbyl-free radical. It is also involved in the first line of antioxidant defense, protecting lipid membranes, and proteins from oxidative damage. As a water-soluble molecule, vitamin C can also work both inside and outside the cells, therefore it can neutralize free radicals.[9] Additionally, vitamin C can prevent free radical induced damage of DNA, which is thought to be an initiating step in cancer formation. Therefore, the possible use of vitamin C in cancer therapy and prevention has been an area of great interest.[37] Vitamin C also can regenerate other antioxidant systems as it is a cofactor for other antioxidants enzymes e.g. vitamin E. Moreover, studies proved that adequate supplementation of vitamin C can spare the utilization and metabolism of tissue vitamin E, increase the effectiveness of vitamin E, and suppress the susceptibility of lipid peroxidation, thereby reducing the risk of pathologic disease due to oxidative stress.[38]

It is concluded that CuO NPs caused toxic effects on the histological structure of the rat spleen. These effects were dose dependent. Administration of vitamin C with CuO NPs had a noticeable protective effect on the histological structure of the spleen in subgroup IIIA which received low dose of NPs. On the other hand, vitamin C showed minimal protective effect when used with high dose of NPs (subgroup IIIB).

CONFLICT OF INTEREST

There are no conflicts of interest.

REFERENCES

1. Zhou M., Tian, M., Li C. Copper-Based Nanomaterials for Cancer Imaging and Therapy. Bioconjugate Chem., 2016; 27: 1188–1199.
2. Vance M., Kuiken T., Vejerano E., McGinnis S., Hochella MF., Rejeski D., Hull MS. Nanotechnology in the real world: Redeveloping the nanomaterial consumer products inventory. Beilstein journal of nanotechnology, 2015; 6: 1769.
3. Frohlich E. and Salar-Behzadi S. Toxicological assessment of inhaled nanoparticles: role of in vivo, ex vivo, in vitro, and in silico studies. Int J Mol Sci., 2014; 15: 4795-4822.
4. Grigore, M., Biscu E., Holban A., Gestal M., Grumezescu, A. Methods of synthesis, properties and biomedical applications of CuO nanoparticles. Pharmaceuticals, 2016; 9(4): 75.
5. Ruiz, P., Katsumiti A., Nieto J.A., Bori J.; Jimeno-Romero A.; et al Short-term effects on antioxidant enzymes and long-term genotoxic and carcinogenic potential of CuO nanoparticles compared to bulk CuO and ionic copper in mussels Mytilus galloprovincialis. Mar. Environ. Res., 2015; 111: 107–120.
6. Gosens I., et al. Organ burden and pulmonary toxicity of nano-sized copper (II) oxide particles after short-term inhalation exposure. Nanotoxicology, 2016; 10: 1084-1095.
7. Cataldi M., Vigliotti C., Mosca T., Cammarota M., Capone D. Emerging role of the spleen in the pharmacokinetics of monoclonal antibodies, nanoparticles and exosomes. International journal of molecular sciences, 2017; 18(6): 1249.
8. Padayatty J., Levine M. Vitamin C: the known and the unknown and Goldilocks. Oral diseases, 2016; 22(6): 463-493.
9. Pehlivan FE., et al; Vitamin C: An Antioxidant Agent. IntechOpen, 2017: (35): 26-27.
10. Teulon M., Godon C., Chantalat L., Moriscot C., Cambedouzou J., Odorico M., Herlin-Boime N. On the Operational Aspects of Measuring Nanoparticle Sizes. Nanomaterials, 2019; 9(1): 18.
11. Privalova L., Katsnelson B., Loginova N., Gurvich V., Shur V., et al; Subchronic toxicity of copper oxide nanoparticles and its attenuation with the help of a combination of bioprotectors. International journal of molecular sciences, 2014; 15(7): 12379-12406.
12. Anreddy RN., et al; Copper oxide nanoparticles induces oxidative stress and liver toxicity in rats following oral exposure. Toxicology reports, 2018; 5: 903-904.
13. Crowley LC, Waterhouse NJ Detecting cleaved caspase-3 in apoptotic cells by flow cytometry. Cold Spring Harbor Protocols, 2016.
14. Bancroft JD, Layton C, Suvarna SK. Bancroft's Theory and Practice of Histological Techniques. 7th ed. Elsevier Churchill Livingstone: London, United Kingdom, 2013; 386–535.
15. Pathakoti, K., Manubolu, M., Hwang, H., Chapter 48-Nanotechnology applications for environmental industry. In Handbook of Nanomaterials for Industrial Applications; Hussain, C.M., Ed.; Elsevier: Cambridge, MA, USA, 2018; 894–907.
16. Dumková J., Smutná T., Vrlíková L., Le Coustumer P., et al: Sub-chronic inhalation of lead oxide nanoparticles revealed their broad distribution and tissue-specific subcellular localization in target organs. Particle and fibre toxicology, 2017; 14(1): 55.
17. Lai X., Zhao H., Zhang Y., Guo K., Xu Y., Chen S., Zhang J. (2018): Intranasal delivery of copper oxide nanoparticles induces pulmonary toxicity and fibrosis in C57BL/6 mice. Scientific reports; 8(1):4499.
18. Yokohira M, et al. (2007): Bioassay by intratracheal instillation for detection of lung toxicity due to fine particles in F344 male rats. Experimental and toxicologic pathology: official journal of the Gesellschaft fur Toxikologische Pathologie; 58:211–221.
19. Sizova EA., Miroshnikov SA., Polyakova VS., Natalia G., Anatoly S., (2012): Copper nanoparticles as modulators of apoptosis and structural changes in tissues. J Biomater Nanobiotechnol; 3: 97-104.
20. Walkey CD., Olsen JB., Guo H., Emili A., Chan WC., (2012): Nanoparticle size and surface chemistry determine serum protein adsorption and

macrophage uptake. Journal of the American Chemical Society; 134(4):2139-47.
21. Wang B., Zhang Y., Mao Z., Yu D., Gao C., (2014): Toxicity of ZnO nanoparticles to macrophages due to cell uptake and intracellular release of zinc ions. Journal of nanoscience and nanotechnology; 14(8):5688-96.
22. Tsugita M., Morimoto N., Nakayama M., (2017): SiO 2 and TiO 2 nanoparticles synergistically trigger macrophage inflammatory responses. Particle and fibre toxicology; 14(1):11.
23. Mazen NF., Saleh EZ., Mahmoud AA., Shaalan AA., (2017): Histological and immunohistochemical study on the potential toxicity of sliver nanoparticles on the structure of the spleen in adult male albino rats. Egyptian Journal of Histology; 40(3):374-87.
24. Yu Y., Duan J., Li Y., Li Y., Jing L., Yang M., Wang J., Sun Z., (2017): Silica nanoparticles induce liver fibrosis via TGF-β1/Smad3 pathway in ICR mice. International journal of nanomedicine; 12:6045.
25. Kumar V., Abbas A., Aster J. (2013): Robbins Basic Pathology. Ninth edition, Philadelphia: Elsevier Inc; 117-120.
26. Cholewińska E., Ognik K., Fotschki B., Zduńczyk Z., Juśkiewicz J., (2018): Comparison of the effect of dietary copper nanoparticles and one copper (II) salt on the copper biodistribution and gastrointestinal and hepatic morphology and function in a rat model. PloS one; 14;13(5):e0197083.
27. Abu-Dief EE, Abdel-Aziz HO, Nor-Eldin EK, Khalil KM, Ragab EE (2018): Ultrastructural, histochemical and biochemical effects of titanium dioxide nanoparticles on adult male albino rat liver and possible prophylactic effects of milk thistle seeds; 1110-0559, Vol. 41, No.1.page 3.
28. Smetana K, Klamova H, Jiraskova I, Hrkal Z. (2008): To the density and distribution of heterochromatin in differentiating, maturing and apoptotic cells represented by granulocytic, lymphocytic and erythrocytic precursors. Folia biologica-praha; 54(1):8.
29. Shubin AV., Demidyuk IV., Komissarov AA., Rafieva LM., Kostrov SV., (2016): Cytoplasmic vacuolization in cell death and survival. Oncotarget; 7(34):55863.
30. Schrand AM., Rahman MF., Hussain SM., Schlager JJ., David A., Smith DA., Syed (2010): Metal-based nanoparticles and their toxicity assessment. Nanomed Nanobiotechnol; 2:544-568.
31. Trickler WJ., Lantz SM., Murdock RC., Schrand AM., Robinson BL., Newport GD., (2010): Silver nanoparticle induced blood-brain barrier inflammation and increased permeability in primary rat brain microvessel endothelial cells. Toxicol Sci; 118:160-70.
32. Cho YM, Mizuta Y, Akagi JI, Toyoda T, Sone M, Ogawa K (2018): Size-dependent acute toxicity of silver nanoparticles in mice. Journal of toxicologic pathology, 31(1): 73-80.
33. Magaye, R., Yue, X., Zou B., Shi H., Yu H., Zhao, J., Acute toxicity of nickel nanoparticles in rats after intravenous injection. International journal of nanomedicine, 2014; 9: 1393.
34. Fukui H., Iwahashi H., Nishio K., Hagihara Y., Yoshida Y., Horie M. Ascorbic acid prevents zinc oxide nanoparticle–induced intracellular oxidative stress and inflammatory responses: Toxicology and industrial health, 2017; 33(9): 687-695.
35. Kong, L., Hu, W., Lu, C., Cheng, K., & Tang, M: Mechanisms underlying nickel nanoparticle induced reproductive toxicity and chemo-protective effects of vitamin C in male rats. Chemosphere, 2019; 218: 259-265.
36. Diab, A. E. A. A., Ibrahim, S. S., ELbahaie, E. S., El Shorbgy, I. M., & Abdel-halim, W. S. Zinc Oxide Nanoparticles-Induced Neurotoxicity And Possible Mitigating Effects Of Artemisia judaica And Vitamin C. Research journal of pharmaceutical biological and chemical sciences, 2018; 9(5): 519-531.
37. Vissers M., Das AB., Potential mechanisms of action for vitamin C in cancer: reviewing the evidence. Frontiers in physiology, 2018; 9: 809.
38. Handana, S. T. P., Andayani, D. E., & Mudjihartini, N: Vitamin E and Vitamin C Intake Among Lactating Mothers In Jakarta. *World Nutrition Journal*, 2019; *3*(1): 28.